Moveout-based wave-equation migration velocity analysis

Yang Zhang and Biondo Biondi

ABSTRACT

We propose a new method to perform wave-equation migration velocity analysis using angle-domain common image gathers. Instead of maximizing the image-stack-power objective function directly with respect to the slowness, we link the objective function to the slowness indirectly through an intermediate moveout parameter. Since this approach is robust against the cycle-skipping problem, it produces more reasonable gradients. Also the proposed method does not require explicit picking of the moveout parameters. Our data examples shows the great potential of this method.

INTRODUCTION

Wave-equation migration velocity analysis (WEMVA) methods aim to utilize velocity information from the migrated images to improve the velocity model. Using the wave equation is potentially more accurate than ray-based methods becuase it better describes wave-propagation physics and will give a more physically realistic senstivity kernel for the velocity update. Evaluating the flatness of the angle-dommain common image gathers (ADCIGs) (Biondi and Symes, 2004) is so far the most favored choice when forming WEMVA optimization problems.

Several WEMVA methods have been proposed, but there is no consensus on the best method. The maximum-stack power method (Chavent and Jacewitz, 1995) directly maximizes the angle stack of the ADCIGs, but similar to the Full Waveform Inversion (FWI) (Tarantola, 1984) method, it is prone to cycle-skipping when the velocity error is too large. The differential-semblance optimization (DSO) (Symes and Carazzone, 1991; Shen et al., 2005; Shen and Symes, 2008) penalizes the first derivative along the angle axis on the ADCIGs. This objective function is easy to implement but will falsely over-penalize an already flat angle gather with variant amplitudes; and the differential operator significantly amplifies the noise in the image, thus generating unwanted artifacts in the velocity upgrade. Sava (2004) uses prestack Stolt residual migration to help construct the image perturbation. The cycle-skipping problem is avoided this way, however the user is required to pick a ρ parameter at each model point, and the picking is not trivial. Furthermore the Stolt migration can only migrate images using constant velocity for the entire velocity model. There

is some question whether the ρ parameters picked with these image-ρ cubes always represent the correct trend of the velocity update.

In this report, we propose a new method which extends from the theory in Biondi (2010, 2011). This method extracts the velocity-focusing information in the angle domain and tries to maximize the angle-stack power of ADCIGs as well. To tackle the cycle-skipping issue, we present a new way to construct the image perturbation by introducing an intermediate moveout parameter that describes the kinematics change of the ADCIGs caused by the velocity change; and that kinematic change then links to the change of objective function. The rest of the paper is divided into two parts: first the theoretical framework is explained; then we demonstrate the effectiveness of our method with several synthetic examples.

THEORY

Practical experience indicates that slowness is a better parameterization than velocity. For clarity, the model space is parameterized as slowness for the rest of the derivation in this paper. To make it simple, the derivation is presented in 2D; however it is straightforward to extend it to three dimensions.

from slowness perturbation to the change in image kinematics

In this section we present the formula that links the slowness perturbation to the shifts of the ADCIGs. Starting from the initial slowness model $s_0(z, x)$, we first define the pre-stack common-image gather in the angle domain as $I(z, \gamma, x; s_0)$, where γ is the reflection angle. If we choose a different slowness $s(z, x)$, the new image $I(z, \gamma, x; s)$ will be different from $I(z, \gamma, x; s_0)$ in terms of both kinematics and amplitude. If, as is commonly done, we focus on the kinematic change, then a way to characterize this kinematic change is to define a shift parameter b at each image location, $b(\gamma, z, x)$, such that if we apply this shift parameter to the initial image, the resulting image $I(z + b, \gamma, x; s_0)$ will agree with the new image $I(z, \gamma, x; s)$ in terms of kinematics. This is indicated by the maximum point of the auxilary objective function:

$$J_{aux}(b) = \int_{-L/2}^{L/2} dz_w \int d\gamma \, I(z + z_w + b, \gamma; z, x, s_0) I(z + z_w, \gamma; z, x, s) \text{ for each x,z.} \quad (1)$$

Note that in order to handle multiple events, we use a local window of length L along the depth axis. For the rest of the paper, the integration bound for variable z_w is always $[-L/2, L/2]$, and each J_{aux} is defined within that window around image point (x,z). $I(z + z_w, \gamma; z, x) = I(z + z_w, \gamma, x)$ represents a windowed version of the entire image.

This methodology is borrowed from Luo and Schuster (1991) who tried to find the relation of the travel-time perturbation to the slowness change. Then $\frac{\partial b}{\partial s}$ can be

found using the rule of partial derivatvies for implicit functions (please refer to the appendix A):

$$\frac{\partial b}{\partial s} = -\frac{\int dz_w\, \dot{I}(z+z_w+b,\gamma;z,x,s_0)\frac{\partial I(z+z_w,\gamma;z,x,s)}{\partial s}}{E(\gamma,z,x)}, \tag{2}$$

in which $E(\gamma,z,x) = \int dz_w \ddot{I}(z+z_w+b,\gamma;z,x,s_0)I(z+z_w,\gamma;x,s)$. $\dot{I}$ and $\ddot{I}$ indicate the first and second derivatives in z (depth). In practice, eq. (2) will be greatly simplified if we evaluate this expression at $s = s_0$, in other words $b = 0$. In fact, this will always be the case if we update the intial slowness s_0 after each iteration. The simplified relation becomes

$$\frac{\partial b}{\partial s}\Big|_{s=s_0} = -\frac{\int dz_w\, \dot{I}(z+z_w,\gamma;z,x,s_0)\frac{\partial I(z+z_w,\gamma;z,x,s)}{\partial s}}{E(\gamma,z,x)}, \tag{3}$$

and the $\frac{\partial I(z+z_w,\gamma;z,x,s)}{\partial s}$ term is indeed the wave-equation image-space tomographic operator. Each part in eq. (3) has clear physical implications: the E term acts as an energy term to normalize the amplitude of the back-projected image; the back-projected image, $\dot{I}(z+z_w,\gamma;z,x,s_0)$ is built based on the initial image; it also has a first-order z derivative that introduces a proper $90°$ phase shift, ensuring a well behaved slowness update from the tomographic operator.
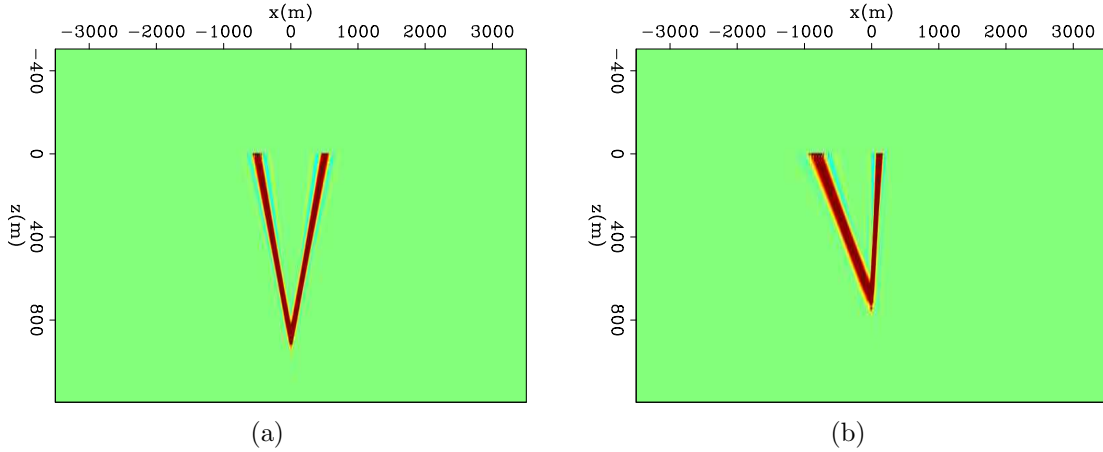

Figure 1: Slowness sensitivity kernel at incident angle $\gamma = 30°$ for a flat reflector (a) and a dipping reflector (b). **[ER]**

For a simple illustration of eq. (3), the slowness sensitivity kernel is calculated, by back-projecting a shift perturbation $\Delta b(\gamma,x)$ that has one single spike at $\gamma = 30°, x = 0$. A uniform background velocity of 2000 m/s is used. Figure 1(a) shows the sensitivity kernel if the reflector is flat, and figure 1(b) shows the sensitivity kernel with a dipping reflector (dip angle $= 20°$). As is clearly shown in these two plots, this operator will project the slowness perturbation along the corresponding wave path based on the location and reflection angle of the image shift.

Introducing the residual moveout parameter

The previous section showed how the slowness change can be associated with the kinematic change of the image. The remaining task is to determine how the image's kinematics should change by evaluating the objective function. Ideally we would like to know the true depth of the reflector, so that we can guarantee that the correct shift direction of the image is extracted. Unfortunately, we usually do not have the true depth of the reflector, and have to find the shift direction by relying only on the flatness criterion. A first attempt that directly maximizes the angle stack after shifting the initial image would be

$$\mathbf{J}(s) = \frac{1}{2} \sum_x \sum_z \int dz_w \left[\int d\gamma\, I(z + z_w + b, \gamma, z, x; s_0) \right]^2. \tag{4}$$

The corresponding derivative over b for a fixed (γ, z, x) is

$$\frac{\partial J}{\partial b(\gamma, z, x)}\big|_{b=0} = \frac{1}{2} \sum_x \sum_z \int dz_w \left\{ \left[\int d\gamma\, I(z + z_w, \gamma, z, x; s_0) \right] \dot{I}(z + z_w, \gamma, z, x; s_0) \right\}. \tag{5}$$

Apparently, this objective function is very susceptible to the cycle-skipping problem: for a fixed (γ, z, x), if the image $I(z + z_w, \gamma, z, x; s_0)$ and the angle-averaged image $\int d\gamma\, I(z + z_w, \gamma, z, x; s_0)$ become out of phase, the derivative of eq. (5) will point to the wrong shift direction.

To prevent cycle-skipping, we need a way to detect the global shape of the AD-CIGs. Almomin (2011) propose to measure the relative shift the traces at each angle with respect to some reference trace by picking cross-correlation peak. Here we use the residual moveout (RMO) parameters so that the objective function knows whether the angle gather is curving up or curving down.

As shown in Biondi (2003) Chap 11, in the case of constant velocity error, the residual moveout of an ADCIG gather is

$$\theta(\gamma) = z_{\rho 0} \frac{\rho - 1}{\cos \alpha_x} \frac{\sin^2 \gamma}{\cos^2 \alpha_x - \sin^2 \gamma},$$

where $\rho = s/s0$, α_x and γ are the dip angle and reflection angle respectively, and z is the true reflector depth, $z_{\rho 0} = z/\rho$. If we assume the dip is small, then the expression above can be further simplified to

$$\theta(\gamma) = z_{\rho 0}(\rho - 1) \tan^2 \gamma.$$

Therefore we introduce the moveout parameter α and the moveout function $g(\gamma) = \tan^2 \gamma$. The objective function we want to maximize is the angle stack-power of the inital image after applying the residual moveout:

$$\mathbf{J} = \frac{1}{2} \sum_x \sum_z \int dz_w \left[\int d\gamma\, I(z + z_w + \alpha g(\gamma), \gamma, z, x; s_0) \right]^2.$$

The derivative is

$$\frac{\partial J}{\partial s}|_{s=s_0} = \sum_x \sum_z \int dz_w \left\{ \left(\int d\gamma I(z + z_w, \gamma, z, x; s_0) \right) \left[\int d\gamma \, \dot{I}(z + z_w, \gamma, z, x; s_0) g(\gamma) \frac{\partial \alpha}{\partial s} \right) \right] \right\}.$$

Define

$$
\begin{aligned}
A(z_w; z, x, s_0) &= \int d\gamma \, I(z + z_w, \gamma; z, x, s_0), \\
B(z_w; z, x, s_0) &= \int d\gamma \, \dot{I}(z + z_w, \gamma; z, x, s_0) g(\gamma),
\end{aligned}
$$

then

$$
\begin{aligned}
\frac{\partial J}{\partial s} &= \sum_x \sum_z \frac{\partial J}{\partial \alpha} \frac{\partial \alpha}{\partial s} \\
&= \sum_x \sum_z \left\{ \int dz_w A(z_w; z, x, s_0) B(z_w; z, x, s_0) \right\} \frac{\partial \alpha}{\partial s}.
\end{aligned}
\tag{6}
$$

We find there are two ways to derive the $\frac{\partial \alpha}{\partial s}$ relation (see appendix B):

1. We can link Δs to $\Delta \alpha$ by defining an auxilary objective function; we call this the *direct operator*.

2. we can convert the perturbation of α to the shift parameter b perturbation at each angle, through a weighted least-squares fitting formula; thus $\Delta \alpha \rightarrow \Delta b \rightarrow \Delta s$; and as shown previously, we know how to calculate $\frac{\partial b}{\partial s}$. We call this the *indirect operator*.

The sensitivity kernel $\frac{\partial \alpha}{\partial s}$ calculated using the direct operator and the indirect operator are shown in figure 2, as with the Toldi operator (Toldi, 1985), the characteristic shape of such a sensitivity kernel is a center lobe, with two side lobes with oppositite polarity, which reaffirms the well known fact that velocity perturbation at the center and the side-end lateral position will change the curvature of ADCIGs towoard opposite directions. Yet the overall average is positive, which would give the correct update in case of a bulk shift slowness error.

Now if we review this method on eq. (6), the success of this method simply relies on the proper behavior of the two components in eq. (6): $\frac{\partial J}{\partial \alpha}$ needs to correctly detect the curvature of the ADCIGs so that the inversion will choose a moveout direction that properly flatten the gathers; $\frac{\partial \alpha}{\partial s}$ needs to properly convert the curvature perturbation to the update in slowness space.

In cases where velocity error is big, the actual curvature of the gather may be poorly represented the $\frac{\partial J}{\partial \alpha}$ term. To further improve the robustness and precondition the gradient, the analytic expression of $\frac{\partial J}{\partial \alpha}$ in eq. (6) is replaced by a numerical approach. First a semblance panel of $J(\alpha)$ will be calculated. To ensure that the derivative at $\alpha = 0$ can determine the correct curvature that maximizes the semblance value, a Gaussian derivative rather than a simple $(-1, 1)$ finite-difference derivative is applied. The width of the Gaussian can be reduced in later iterations.
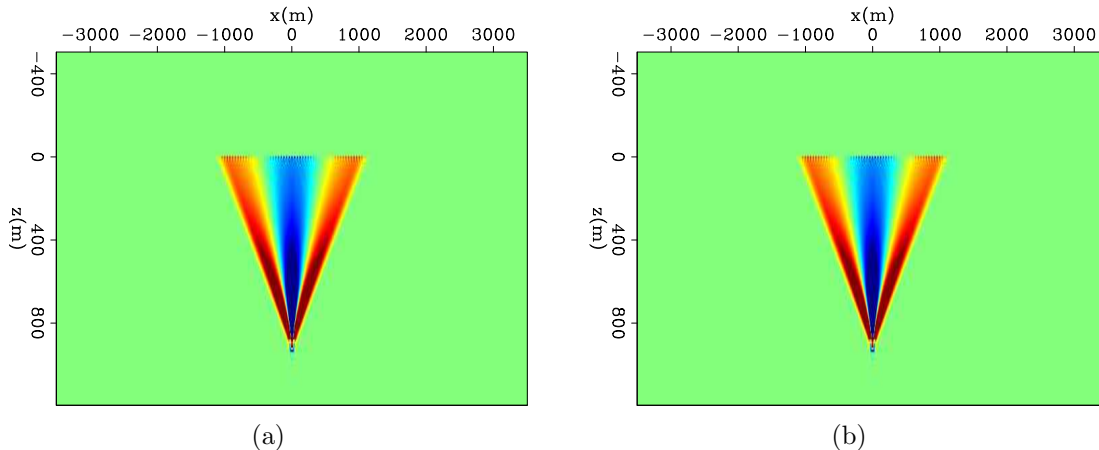
Figure 2: Sensitivity kernel $\partial\alpha/\partial s$ calulated using the direct operator (a) and the indirect operator (b), using constant background velocity and a flat reflector. [**CR**]

RESULTS

We create several synthetic examples to show the effectiveness of our method. The model is 16 km in x and 1.2 km in z. The grid sampling is 20 m in x and 10 m in z. The survey geometry follows the marine acquisition convention with 4km cable length, receiver spacing is 20 m and a total of 150 shots are simulated from -6 km to +6 km with a spacing of 80 m. A total of 106 frequencies are calculated, ranging from 5 Hz to 40 Hz. Unless explicitly mentioned, there is one flat reflector at a depth around 800 m and a constant background velocity of 2000 m/s is used. A one-way propagator is used for computational efficiency. For comparison, the subsurface-offset DSO and straight maximum-stack-power method are also implemented.

The first example is a true velocity with a 1 km width Gaussian anomaly at the center, with peak value 4000 m/s. Figure 3(a) shows the anomaly (in slowness) and Fig 3(b) shows the migrated zero subsurface-offset image, The velocity error is so large that the center part of the reflector is pulled up significantly.

Figure 4 shows the first slowness update using the three methods. Our method presents the most pleasing update among the three; the location of the anomaly is correctly located, and the target region is more uniformly updated, except for the small holes within the "W" shape due to the poorer wave path coverage caused by the curved reflector. The DSO result shows the typical strip-shaped artifacts, and the amplitude of the target region is weak compared to the edge artifacts. The maximum-stack-power method suffers from cycle skipping and is not able to locate the target area.

In the second example the true velocity has a horizontal gradient, where velocity increase linearly from 1500 m/s to 2700 m/s. Figure 5(a) shows the true model (in slowness) and figure 5(b) shows the migrated zero subsurface-offset image. The originally flat reflector is tilted in the image because of the horizontal slowness gradient.
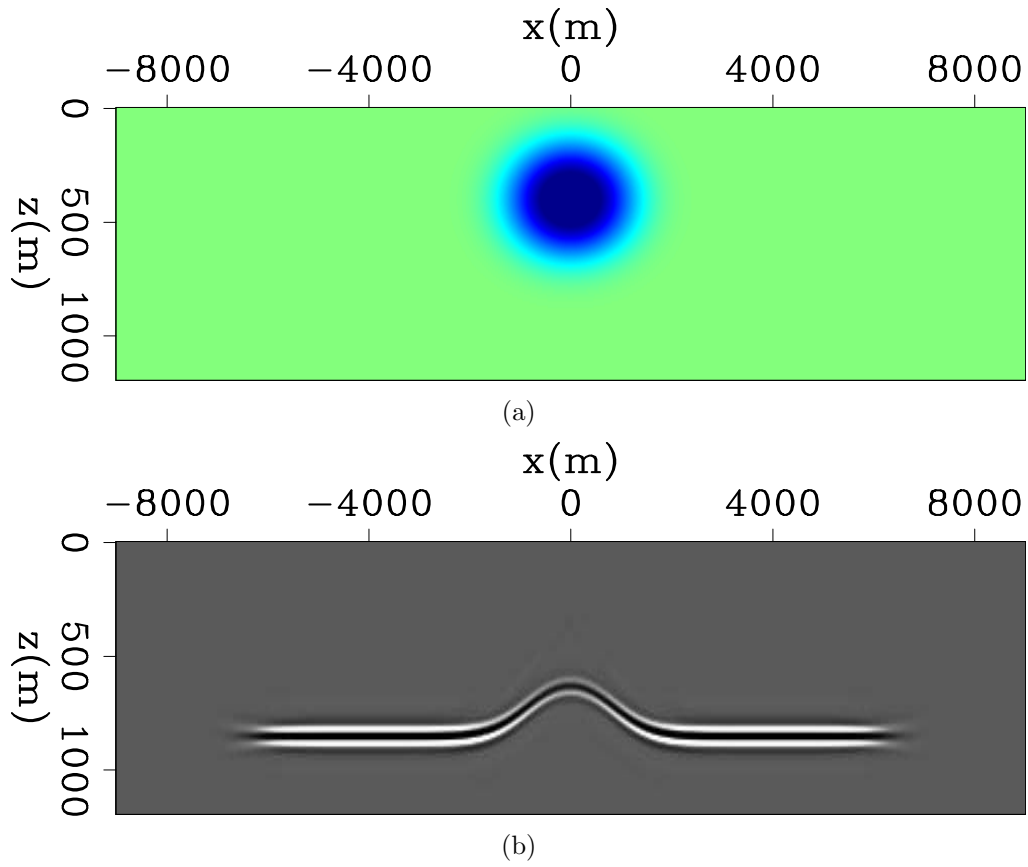
(a)

(b)

Figure 3: (a) The slowness model with a Gaussian anomaly.   [**NR**](b) The migrated image using constant background slowness.   [**CR**]
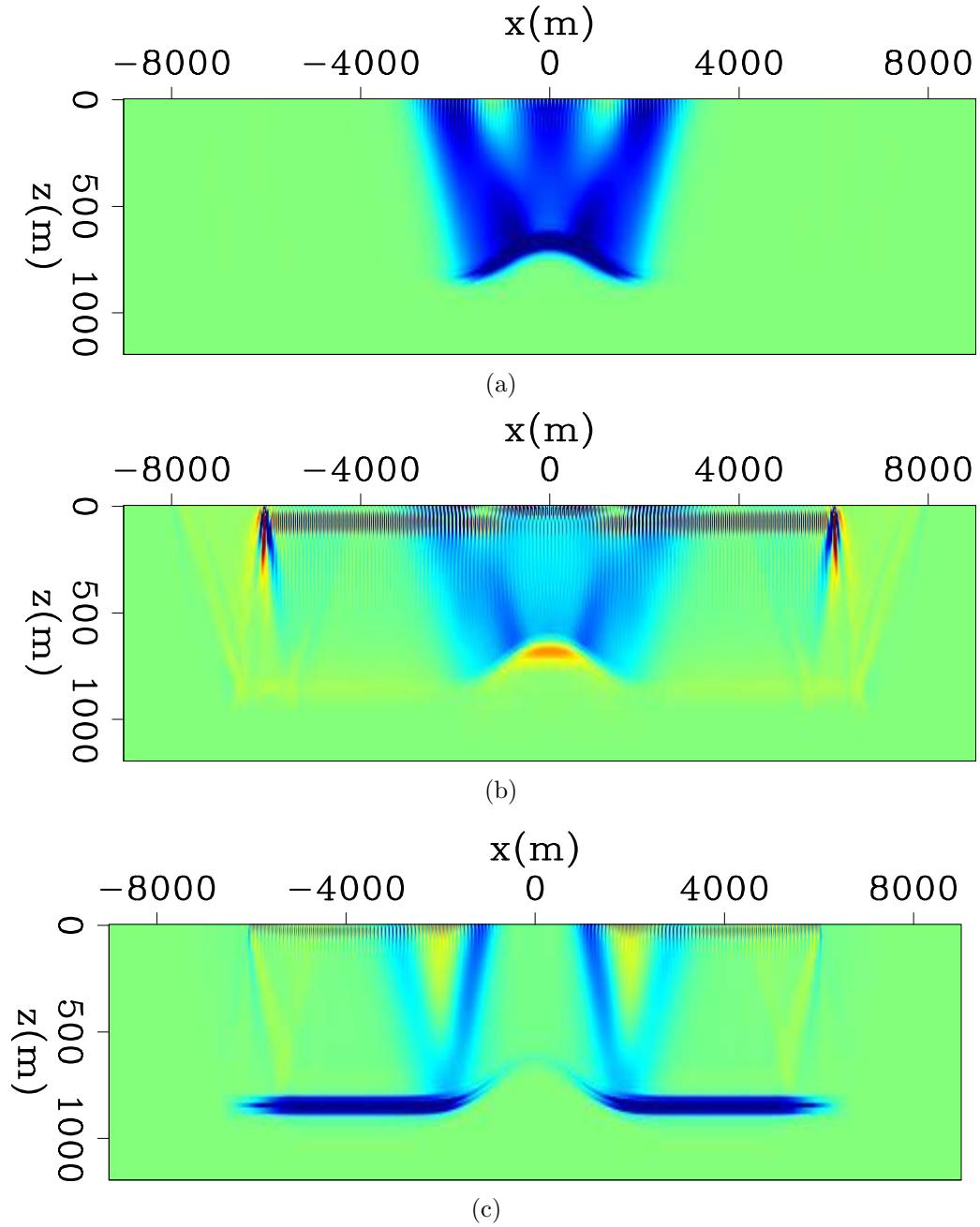
(a)

(b)

(c)

Figure 4: The first slowness update direction of our method (a), the subsurface-offset domain DSO (b), and the direct stack-power-maximization (c), true slowness refers to figure 3(a). [**CR**]
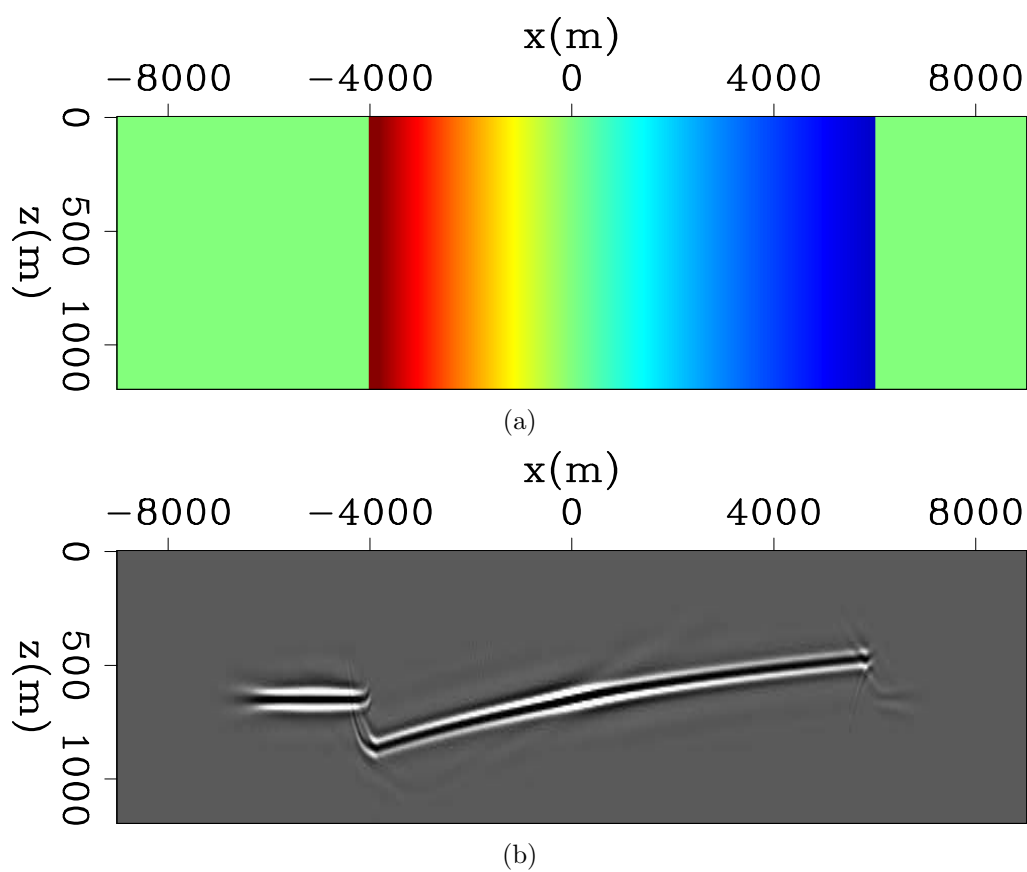
(a)

(b)

Figure 5: (a) The slowness model with a horizontal gradient from 1500m/s to 2700m/s [**NR**];(b) The migrated image using constant background slowness.   [**CR**]
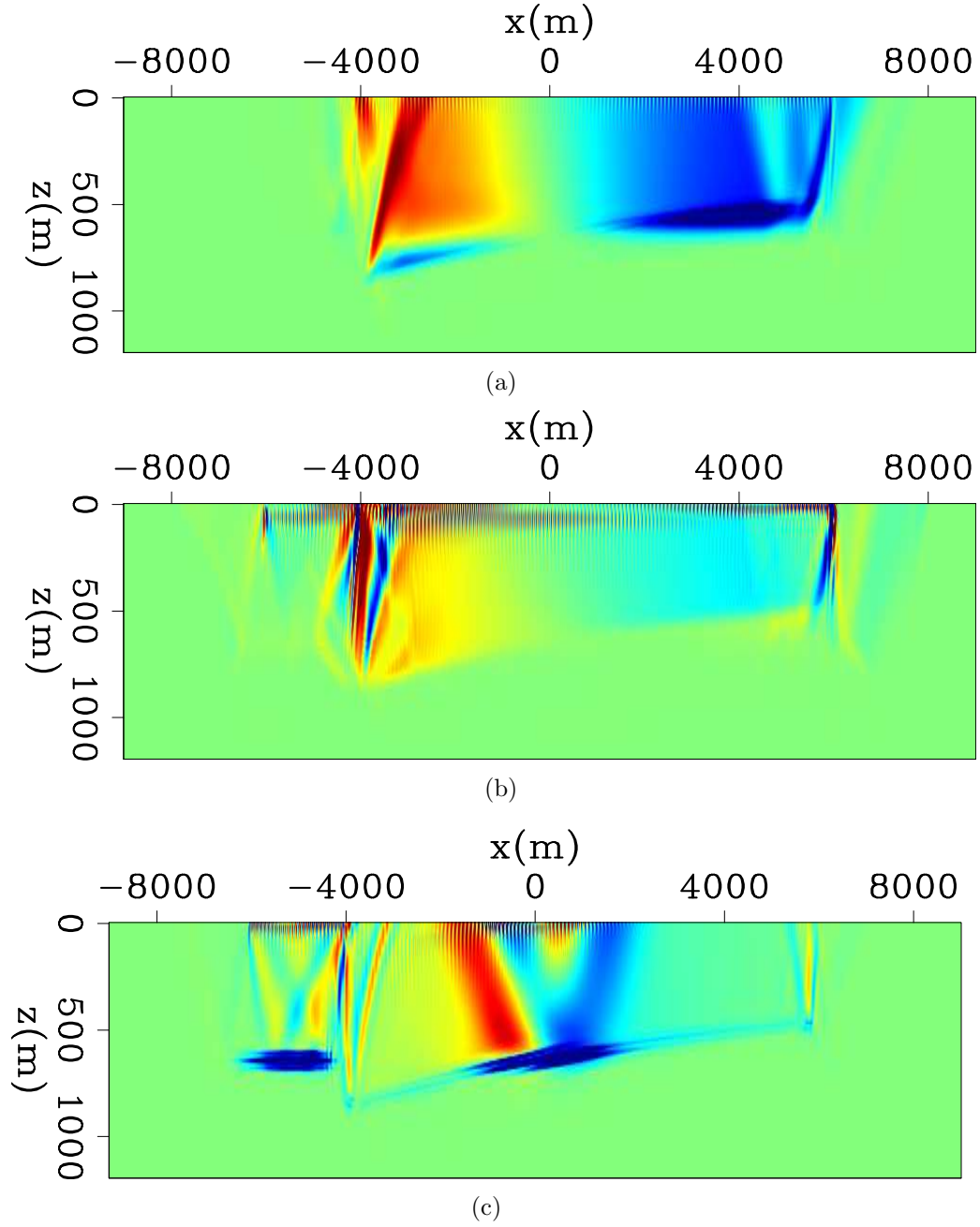
(a)

(b)

(c)

Figure 6: The first slowness update direction of our method (a), the subsurface-offset domain DSO (b), and direct stack power maximization (c). The true slowness refers to figure 5(a). **[CR]**

Figure 6 shows the first slowness update using the three methods. Again our method presents the most pleasing update among the three. The amplitude of the search direction is proportional to the actual magnitude of the slowness error. A large strip-shaped artifact is introduced at $x = -4000\,m$ in DSO update. this is commonly seen from DSO results when there are reflector discontinuities; although it does decently predicted the horizontal gradient shape of the slowness error. The maximum-stack-power method is able to predict correctly when the slowness error is small (around $x = 0\,m$). As the slowness error reaches a certain threshold, cycle-skipping happens and the result deteriorates.

For the third example, the true velocity is a constant $1900\,m/s$ plus a high veloicty anomaly at $x = 2000\,m/s$ with peak value $2850\,m/s$. We designed a hump-shaped reflector to test this method's ability to handle mild dips. Figure 7(a) shows the true model (in slowness) and Fig 7(b) shows the migrated zero subsurface-offset image. Figure 7(c) and 7(d) shows the first slowness update using our method and the DSO method. The effect of the high velocity anomaly is partially cancelled by the lower constant part ($1900\,m/s$), nontheless, the overall result still requires a negative update at the anomaly's location. In the presence of a mild dipping reflector, our method still yields a satisfying result.

The effect of the high velocity anomaly is partially cancelled by the lower constant part ($1900\,m/s$), nontheless, the overall result still requires a negative update at the anomaly's location. In the presence of a mild dipping reflector, our method still yields a satisfying result.

Based on the gradient calculation, we implement an non-linear slowness inversion framework. The example we tested is the marmousi velocity model. The model is $6\,km$ in x and $1.6\,km$ in z. The spatial sampling is $20\,m$. The survey geometry follows the land acquisition convention with receiver at every surface location on the top and a total of 51 shots are simulated covering the whole lateral span on the top with a spacing of $120\,m$.

Figure 8(a) shows the true model (in velocity) and figure 8(b) shows the starting model, which has a vertical gradient increasing from $1600\,m/s$ to $3200\,m/s$. Figure 8(c) and 8(d) show the inverted velocity model using our method and subsurface-offset DSO method. We run 20 nonlinear iterations for each inversion, and the same extent of gradient smoothing is applied. Although both inversion result improves the focusing of the subsurface-offset image, the outline of the true velocity structure is much better captured with our method.

CONCLUSION

We present a new method to perform wave-equation migration velocity analysis. It properly captures the kinematic update from the ADCIGs and projects that update into the slowness space. We demonstrated this promising approach using several examples. As shown previously, this method does not suffer from cycle-skipping,
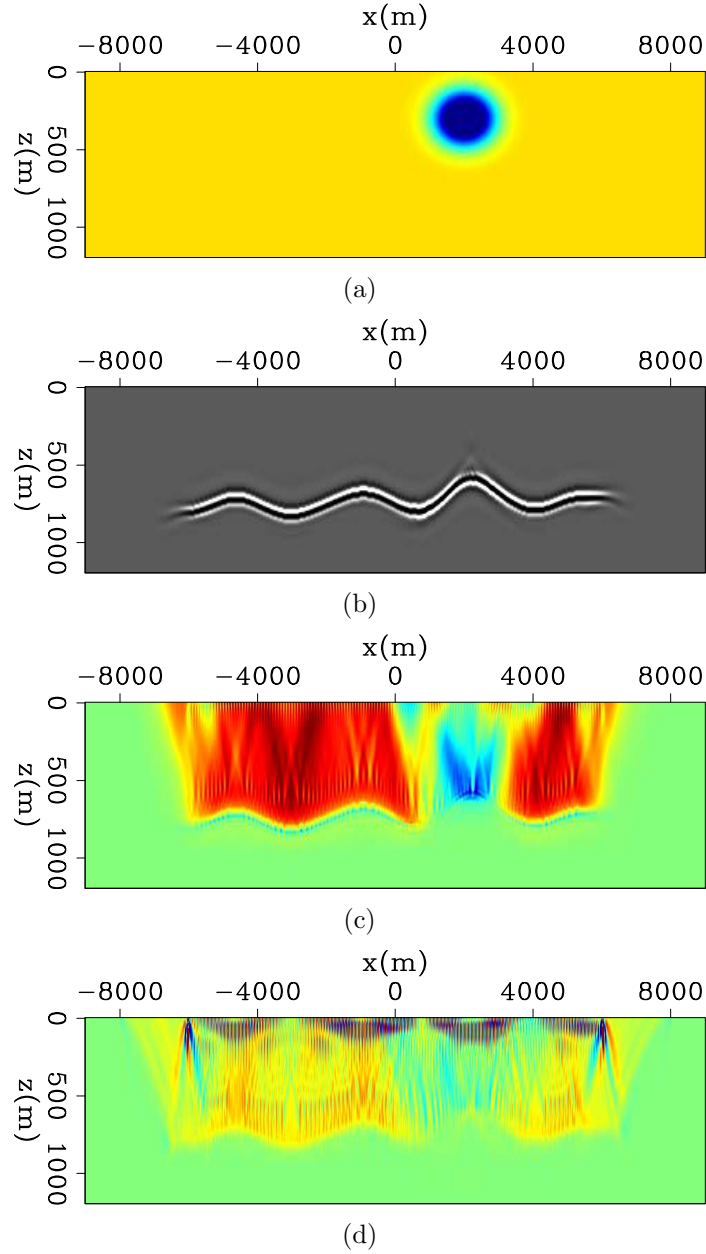
Figure 7: (a) The slowness model with a constant slower velocity $1900\,m/s$, there is also a high velocity anomaly at $x = 2000\,m$, with peak value $2850\,m/s$; [**NR**](b) The migrated image using constant background velocity $(2000\,m/s)$. [**CR**](c) The first slowness update direction using our method; [**CR**](d) The first slowness update using the subsurface-offset domain DSO method. [**CR**]
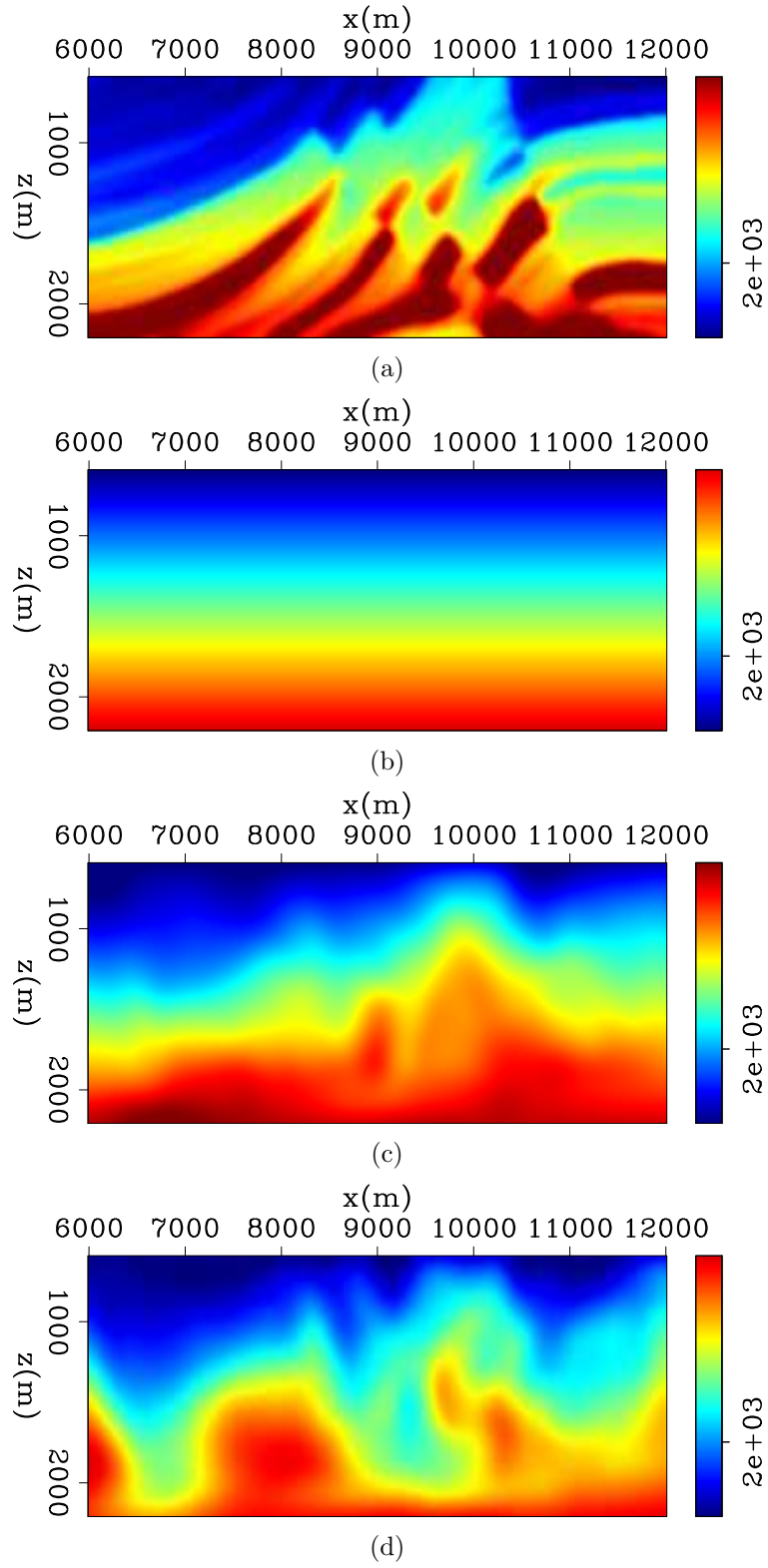
Figure 8: The true velocity model of Marmousi (a) (slightly smoothed) [**NR**]; the starting velocity model (b) [**NR**]; the inverted velocity model using our method (c) and using the subsurface-offset DSO (d). [**CR**]

does not require moveout parameters picking, and can robustly improve the flatness of the angle gathers. We plan to further develop this method and apply it to more challenging data.

ACKNOWLEDGEMENT

REFERENCES

Almomin, A., 2011, Correlation-based wave-equation migration velocity analysis: SEP-Report, **143**, X–Y.

Biondi, B., 2003, 3-D Seismic Imaging: SEG.

———, 2010, Wave-equation migration velocity analysis by residual moveout fitting: SEP-Report, **142**.

———, 2011, Migration velocity analysis by one-parameter residual moveout fitting in presence of strong lateral velocity anomalies: SEP-Report, **143**, X–Y.

Biondi, B. and W. W. Symes, 2004, Angle-domain common-image gathers for migration velocity analysis by wavefield-continuation imaging: Geophysics, **69**, 1283–1298.

Chavent, G. and C. A. Jacewitz, 1995, Determination of background velocities by multiple migration fitting: Geophysics, **60**, 476–490.

Luo, Y. and G. T. Schuster, 1991, Wave-equation traveltime inversion: Geophysics, **56**, 645–653.

Sava, P., 2004, Migration and Velocity Analysis by Wavefield Extrapolation: PhD thesis, Stanford University.

Shen, P. and W. W. Symes, 2008, Automatic velocity analysis via shot profile migration: Geophysics, **73**, VE49–VE59.

Shen, P., W. W. Symes, S. Morton, A. Hess, and H. Calandra, 2005, Differential semblance velocity analysis via shot profile migration: SEG Technical Program Expanded Abstracts, **24**, 2249–2252.

Symes, W. W. and J. J. Carazzone, 1991, Velocity inversion by differential semblance optimization: Geophysics, **56**, 654–663.

Tarantola, A., 1984, Inversion of seismic reflection data in the acoustic approximation: Geophysics, **49**, 1259–1266.

Toldi, J., 1985, Velocity analysis without picking: PhD thesis, Stanford University.

APPENDIX-A

Details of the $\frac{\partial b}{\partial s}$ sensitivity kernel calculation

This section illustrates how to calculate the sensitivity kernel of the image shift parameter $b(\gamma, x)$: $\frac{\partial b}{\partial s}$. Since b maximizes the auxillary objective function,

$$J_{aux}(b) = \int dz_w \int d\gamma \, I(z + z_w + b, \gamma; z, x, s_0)I(z + z_w, \gamma; z, x, s) \text{ for each z,x,} \quad (7)$$

we have

$$\frac{\partial J_{aux}}{\partial b} = 0. \quad (8)$$

To find the relation between b and $s(x)$, we differentiate equation (8) with respect to b and s, which yields

$$\frac{\partial^2 J_{aux}}{\partial b^2} \frac{\partial b}{\partial s} = -\frac{\partial J_{aux}}{\partial b \partial s}, \quad (9)$$

in which we can find

$$\frac{\partial J_{aux}}{\partial b} = \int dz_w \dot{I}(z + z_w + b, \gamma; z, x, s_0)I(z + z_w, \gamma; z, x, s),$$

$\dot{I}, \ddot{I}$ indicate the first and second derivatives in z (depth). Let

$$\frac{\partial^2 J_{aux}}{\partial b^2} = \int dz_w \, \ddot{I}(z + z_w + b, \gamma; x, z, s_0)I(z + z_w, \gamma; x, z, s) = E(x, z).$$

Then substituting the above two equations into eq. (9) leads to

$$\frac{\partial b}{\partial s} = -\frac{\int dz_w \, \dot{I}(z + z_w + b, \gamma; z, x, s_0)\frac{\partial I(z+z_w, \gamma; z, x, s)}{\partial s}}{E(\gamma, z, x)}, \quad (10)$$

which is eq. (2).

APPENDIX-B

Details of $\frac{\partial \alpha}{\partial s}$ sensitivity kernel calculation

This section provides the derivation of the *direct* $\frac{\partial \alpha}{\partial s}$ operator. The approach is to define the auxilary function that links moveout parameter $\alpha(z, x)$ and the slowness s.

$$J_{aux} = \int dz_w \int d\gamma \, I(z + z_w + \theta(\alpha, \beta, \gamma), \gamma; z, x, s_0)I(z, \gamma; z, x, s) \text{ for each z,x ,} \quad (11)$$

in which

$$\theta(\alpha, \beta, \gamma) = \alpha \tan^2 \gamma + \beta = \alpha g(\gamma) + \beta h(\gamma).$$

Notice that here the moveout between the initial image $I(s_0)$ and the new image $I(s)$ is characterized by *both curvature α and constant shift β*. The β parameter does **not** affect the gather flatness; therefore there is no need to put it into the objective function in () , however β is essential to describe the change of image's kinematics.

Since α, β maximize eq (11),

$$\left\{ \begin{array}{l} \frac{\partial J_{aux}}{\partial \alpha} = 0 \\ \\ \frac{\partial J_{aux}}{\partial \beta} = 0 \end{array} \right. . \tag{12}$$

We differentiate the equation (12) with respect to α, β and s, which gives

$$\left[\begin{array}{cc} \frac{\partial^2 J_{aux}}{\partial \alpha^2} & \frac{\partial^2 J_{aux}}{\partial \alpha \partial \beta} \\ \\ \frac{\partial^2 J_{aux}}{\partial \alpha \partial \beta} & \frac{\partial^2 J_{aux}}{\partial \beta^2} \end{array} \right] \left[\begin{array}{c} \frac{\partial \alpha}{\partial s} \\ \\ \frac{\partial \beta}{\partial s} \end{array} \right] = - \left[\begin{array}{c} \frac{\partial J_{aux}}{\partial \alpha \partial s} \\ \\ \frac{\partial J_{aux}}{\partial \beta \partial s} \end{array} \right] . \tag{13}$$

Now we need to invert a Jacobian to get $d\alpha/ds$. We define the following:

$$\frac{\partial^2 J_{aux}}{\partial \alpha^2} = \int dz_w \int d\gamma \, \ddot{I}(z + z_w + \theta, \gamma; z, x, s_0) g^2(\gamma) I(z + z_w, \gamma; z, x, s) = \quad E_{11}(z, x)$$

$$\frac{\partial^2 J_{aux}}{\partial \alpha \partial \beta} = \int dz_w \int d\gamma \, \ddot{I}(z + z_w + \theta, \gamma; z, x, s_0) g(\gamma) h(\gamma) I(z + z_w, \gamma; z, x, s) = \quad E_{12}(z, x)$$

$$\frac{\partial^2 J_{aux}}{\partial \beta^2} = \int dz_w \int d\gamma \, \ddot{I}(z + z_w + \theta, \gamma; z, x, s_0) h^2(\gamma) I(z + z_w, \gamma; z, x, s) = \quad E_{22}(z, x)$$

$$\tag{14}$$

Let the inverse of matrix E to be matrix F:

$$F = \left[\begin{array}{cc} F_{11} & F_{12} \\ F_{12} & F_{22} \end{array} \right] = \left[\begin{array}{cc} E_{11} & E_{12} \\ E_{12} & E_{22} \end{array} \right]^{-1}$$

Then

$$\frac{\partial \alpha}{\partial s} \Big|_{s=s_0} = - \int dz_w \int d\gamma (F_{11} g(\gamma) + F_{12} h(\gamma)) \dot{I}(z + z_w, \gamma; z, x, s_0) \frac{\partial I(z + z_w, \gamma; z, x, s)}{\partial s}. \tag{15}$$

There is another way to define the relation between α and s, leading to the *indidirect* $\frac{\partial \alpha}{\partial s}$ operator using a weighted least-squares fitting formula. Suppose we have the locations of one event in the ADCIGs at location (γ_i, z_i), and we introduce a moveout formula $\theta(\gamma) = z_0 + \alpha \tan^2 \gamma$. Now we define the best fitted intercept and curvature (z_0 and α) values as follows:

$$(z_0, \alpha) = \arg \min_{z_0, \alpha} \sum_i \{(z_i - \alpha \tan^2 \gamma_i - z_0)^2 w_i^2\}, \tag{16}$$

where w_i is the energy of the event at angle γ_i, serving as a weight for the least-squares fitting. We denote $\overline{x} = \sum_i x_i w_i^2$ (the weighted average of quantity x), then

$$\alpha = \frac{\overline{1}\,\overline{(z \tan^2 \gamma)} - \overline{\tan^2 \gamma}\,\overline{z}}{\overline{1}\,\overline{\tan^4 \gamma} - (\overline{\tan^2 \gamma})^2}.$$

It is easy to find $\Delta \alpha$ if there is a pertubation of b_i on z_i:

$$\frac{\partial \alpha}{\partial b_i} = \frac{w_i^2 (\overline{1}\,\tan^2 \gamma_i - \overline{\tan^2 \gamma})}{\overline{1}\,\overline{\tan^4 \gamma} - (\overline{\tan^2 \gamma})^2} \ . \tag{17}$$

Finally,

$$\frac{\partial \alpha}{\partial s} = \sum_i \frac{\partial \alpha}{\partial b_i}\frac{\partial b_i}{\partial s}, \tag{18}$$

where $\frac{\partial \alpha}{\partial b_i}, \frac{\partial b_i}{\partial s}$ are defined respectively in equations (17) and (10).